Journal Pre-proof

Synthesis of feldspathoids and zeolite K–F from waste amber container glass

Jessica H. Taylor, Victoria K. Elmes, Andrew P. Hurt, Nichola J. Coleman

Please cite this article as: J.H. Taylor, V.K. Elmes, A.P. Hurt, N.J. Coleman, Synthesis of feldspathoids and zeolite K–F from waste amber container glass, *Materials Chemistry and Physics* (2020), doi: https://doi.org/10.1016/j.matchemphys.2020.122805.

This is a PDF file of an article that has undergone enhancements after acceptance, such as the addition of a cover page and metadata, and formatting for readability, but it is not yet the definitive version of record. This version will undergo additional copyediting, typesetting and review before it is published in its final form, but we are providing this version to give early visibility of the article. Please note that, during the production process, errors may be discovered which could affect the content, and all legal disclaimers that apply to the journal pertain.

Synthesis of feldspathoids and zeolite K-F from waste amber container glass

Jessica H. Taylor, Victoria K. Elmes, Andrew P. Hurt, Nichola J. Coleman*

School of Science, University of Greenwich, Chatham Maritime, Chatham, Kent, ME4 4TB, UK

*Corresponding author. E-mail address: n.coleman@gre.ac.uk

Declarations of interest: none.

ABSTRACT

The hydrothermal formation of mineral products from a mixture of amber container glass and aluminium waste (Al:Si = 1) in 4 M $NaOH_{(aq)}$ or 4 M $KOH_{(aq)}$ at 100 °C was monitored at 1, 3 and 10 days by X-ray diffraction analysis with Rietveld refinement, Fourier transform infrared spectroscopy and scanning electron microscopy with energy dispersive X-ray analysis. In $NaOH_{(aq)}$, at 1, 3 and 10 days, respectively, 48%, 55% and 63% of the glass crystallised to form hydroxysodalite (HS) and hydroxycancrinite (HC) with minor proportions of katoite and tobermorite. The partial successive transformation of HS to HC was also observed with time. The initial rates of dissolution of the glass and formation of the principal zeolite K-F and secondary katoite phases were considerably slower in $KOH_{(aq)}$; although, the subsequent development of the products was greater than that in $NaOH_{(aq)}$. The zeolite K-F product achieved only 5% crystallinity within the first day which then increased markedly to 60% and 78% at 3 and 10 days, respectively. Despite the incomplete conversion of amber glass into crystalline zeolitic phases, the uptake capacities of the 10-day feldspathoid and zeolite K-F products for Pb^{2+} (4.3 and 4.5 meq g^{-1}, respectively) and Zn^{2+} (3.9 and 4.1 meq g^{-1}, respectively) ions compared favourably with those of many other zeolites and waste-derived inorganic sorbents reported in the literature.

Keywords: Sodalite, Cancrinite, Zeolite K-F, Ion-exchange, Hydrothermal synthesis

1. Introduction

The manufacture of soda-lime-silica container glass for bottled beverages is an energy-intensive process with a relatively high carbon footprint [1-3]. The average primary energy consumption for container glass produced from 50% recycled cullet is currently estimated to be 5.15 MJ kg^{-1} and a carbon footprint of 150-761 kgCO$_2$e *per* 1,000 litres of beverage is associated with the lifecycle of glass bottles [1-3]. Partial replacement of recycled cullet in the glass-making process reduces both energy requirement and unwanted emissions, although the potential to recycle coloured container glass is limited by various technical, economic and societal factors [4]. For example, effective collection, separation and subsequent recycling of green and amber soda-lime-silica glass bottles are essentially restricted to regions with established beer- and wine-making industries.

The major oxide constituents of flint and coloured soda-lime-silica container glasses are SiO$_2$ (70-75 wt%), Na$_2$O (13-17 wt%) and CaO (5-10 wt%) with minor oxide components (Al$_2$O$_3$, MgO, and K$_2$O) below 5 wt% and trace oxides (e.g. Fe$_2$O$_3$, SO$_3$ and Cr$_2$O$_3$) below 0.5 wt% [5,6]. In this respect, surplus coloured container glass represents a consistent source of reactive silica with negligible concentrations of potentially hazardous elements in comparison with other silicate-bearing wastes such as incineration ashes and slags [7-9].

Recently, a range of initiatives to convert waste container glass into value-added materials such as ceramics, geopolymers, ion-exchangers, sorbents and catalysts has been reported in the literature [6-15]. In particular, the synthesis of zeolites and feldspathoids from waste container glass is of current relevance as these 3-D microporous aluminosilicate framework materials find wide application in separation and adsorption technology, soil fertilisation and conditioning, animal feed, construction and catalysis [6-9,15]. Typically, stoichiometric additions of an aluminium-bearing reagent are combined with ground waste

glass which is then subjected to hydrothermal processing under alkaline conditions to produce an assemblage of zeolitic phases. To date, various mixtures of synthetic sodalite, cancrinite, analcime (analcite), faujasite (zeolite X), gismondine (zeolite P), edingtonite (zeolite F) and zeolite A structures have been prepared from container glass using convection and microwave heating [6-9,15]. Phase-pure zeolite products are rarely formed from particulate waste materials in the absence of preconditioning stages (to remove unwanted species and/or produce an homogeneous precursor gel) and templating molecules or nucleating agents [6-9,15]. Phase-pure zeolites are required in some biomedical, chemical and separation processes, although mixtures of impure zeolitic phases are often suitable for many industrial and agricultural applications.

Sodalite and cancrinite are naturally occurring feldspathoid minerals that have different structural frameworks, although share the same chemical formula, $Na(Al_6Si_6O_{24}).2NaX.6H_2O$, where X can be various anions [16]. Their industrial significance in adsorption and separation processes arises from their high ion-exchange capacities and ultramicroporosities. Sodalite and cancrinite are common target phases for the recycling of calcium-bearing aluminosilicate industrial wastes as, unlike many zeolitic materials, they tolerate the substitution of two Na^+ ions for one Ca^{2+} ion during synthesis [6,17].

Zeolite K-F ($K_2Al_2Si_3O_{10}.xH_2O$) is a synthetic analogue of edingtonite ($BaAl_2Si_3O_{10}.4H_2O$), first reported in the 1950s and subsequently prepared from colloidal silica [18], kaolin [19], K-feldspar [20] and incineration ashes of rice husk [21], coal [22] and paper sludge [23]. Current interest in the facile and economical synthesis of zeolite K-F arises from its applications in soil fertilisation and conditioning [19-23].

The present study explores the potential of waste amber container glass to be used as a feedstock (in combination with waste aluminium foil) for the hydrothermal synthesis of a mixture of feldspathoids (hydroxysodalite and hydroxycancrinite) in $NaOH_{(aq)}$ and zeolite K-

F in KOH$_{(aq)}$ at 100 °C. The phase evolution and crystallinity of the hydrothermal reaction products were monitored at 1, 3 and 10 days by powder X-ray diffraction analysis (XRD). The reaction products were also characterised by Fourier transform infrared spectroscopy (FTIR), ^{29}Si and ^{27}Al magic angle spinning nuclear magnetic resonance spectroscopy (MAS NMR) and scanning electron microscopy (SEM) with energy dispersive X-ray analysis (EDX). The uptakes of Pb^{2+} and Zn^{2+} ions by the 10-day feldspathoid and zeolite K-F products were evaluated by batch sorption and compared with those of other waste-derived sorbents and ion-exchangers.

2. Materials and methods

2.1 Preparation of feldspathoid and zeolite products

Discarded amber soda-lime-silica glass beer bottles and aluminium foil were recovered from the municipal waste stream in Chatham, Kent, UK. The bottles were rinsed with water to remove paper labels and ground in a ball mill to pass 125 μm. Quantitative analysis of the amber glass (Table 1) was obtained by X-ray fluorescence spectroscopy at the Materials Research Institute, Sheffield Hallam University, Sheffield, UK. All other reagents were purchased from Sigma-Aldrich, UK, and were used without further purification or modification.

Table 1. Oxide and elemental compositions of amber container glass.

Oxide component	Mass (%)	Mole (%)	Element	Mass (%)	Mole (%)
SiO_2	70.82	71.33	Si	33.11	24.53
Na_2O	13.75	13.43	Na	10.20	9.23
CaO	10.03	10.82	Ca	7.17	3.72
Al_2O_3	2.21	1.31	Al	1.17	0.90
MgO	1.42	2.13	Mg	0.86	0.73
K_2O	0.87	0.56	K	0.72	0.38
Fe_2O_3	0.43	0.16	Fe	0.30	0.11
SO_3	0.31	0.23	S	0.12	0.08
Cr_2O_3	0.04	0.02	Cr	0.03	0.01
-	-	-	O	46.36	60.28
Total	99.9	100	Total	100	100

The mixed hydroxysodalite and hydroxycancrinite feldspathoid products were prepared by modifying the method described in reference 6. In each case, a solution containing 0.90 g of waste aluminium foil dissolved in 15 cm^3 of 4M NaOH$_{(aq)}$ was contacted with 3.0 g of ground amber glass and the resulting mixture was heated at 100 °C in an hermetically sealed 150 cm^3 PTFE reaction vessel. These proportions of amber glass and aluminium foil were selected to provide equimolar quantities of silicon and aluminium in the reaction mixture (*i.e.* 0.035 mol) as the molar Al:Si ratio of the target feldspathoid products is 1:1. Samples N-1, N-3 and N-10 were prepared in triplicate by heating the mixture for 1, 3 and 10 days, respectively. Zeolite K-F was prepared similarly by heating 3.0 g of ground amber glass with a solution containing 0.90 g of waste aluminium foil dissolved in 15 cm^3 of 4M KOH$_{(aq)}$ at 100 °C. Samples K-1, K-3 and K-10 were prepared in triplicate for 1, 3 and 10 days, respectively. All hydrothermal reaction products were recovered by gravitational filtration, washed with deionised water to pH 8, dried to constant mass in air at 40 °C and stored in air-tight polypropylene containers prior to analysis.

2.2 Characterisation of feldspathoid and zeolite products

The hydrothermal reaction products were analysed by powder XRD using a Bruker D8 diffractometer with Cu Kα = 1.5406 Å, a step size of 0.019° in the 2θ range from 2 to 60 ° and a measuring time of 1 s *per* step. The degree of crystallinity of the samples was estimated from the ratio of the area of the crystalline peaks to the total area of the pattern using Bruker EVA version 5.1 software. The weight fractions of the crystalline phases were obtained by Rietveld refinement using Bruker TOPAS version 5.0 software [24]. FTIR spectra were acquired using a Perkin Elmer Spectrum Two spectrometer between 500 and 2000 cm^{-1} wavenumbers, with 10 scans at a resolution of 4 cm^{-1}. Secondary electron images of the

6

products were obtained from uncoated samples attached to carbon tabs on an Hitachi SU8030 scanning electron microscope with an accelerating voltage of 1 kV. EDX data were collected in quintuplicate from areas of 100 μm^2 using a JEOL JSM-5410 LV electron microscope with an Oxford Instruments X-MaxN EDX detector in low vacuum mode with an accelerating voltage of 8 kV. The specific surface areas of the ground amber glass and hydrothermal reaction products were obtained by nitrogen gas sorption analysis *via* the BET method using a Micromeritics Gemini VII gas sorption analyser [25]. Prior to gas sorption, the samples were degassed overnight at 40 °C under flowing nitrogen. BET isotherms were collected in triplicate for each sample. MAS NMR spectra of the amber container glass, sample N-10 and sample K-10 were collected on a JEOL JNM-ECX 300 MHz spectrometer. Single pulse ^{29}Si MAS NMR spectra were obtained with a pulse delay of 60 s, an acquisition time of 0.02048 s and a minimum of 20 000 scans. Single pulse ^{27}Al MAS NMR spectra were obtained with a pulse delay of 0.5 s, an acquisition time of 0.01024 s and 7000 scans. ^{29}Si and ^{27}Al chemical shifts were referenced to tetramethylsilane (TMS) and the aluminium hexaquo ion $[Al(H_2O)_6]^{3+}$, respectively. The common notation used to interpret the ^{29}Si MAS NMR spectra and to describe the local silicate environments in the amber glass and hydrothermal products is such that the symbol Q represents one SiO_4^{4-} tetrahedron and the superscript, n, denotes the number of other Q units to which it is bonded *via* Si-O-Si linkages. For example, a midchain SiO_4^{4-} unit linked to two other SiO_4^{4-} units is represented as Q^2, and a branching SiO_4^{4-} unit linked to two other SiO_4^{4-} units and one AlO_4^{5-} unit is denoted by $Q^3(1Al)$.

2.3 Uptake of Pb^{2+} and Zn^{2+} ions by feldspathoid and zeolite products

The removal of Pb^{2+} and Zn^{2+} from aqueous solutions by the N-10 and K-10 products was determined by single metal batch sorption experiments. In each case, 0.10 g of N-10 or

K-10 were contacted with 0.2 dm^3 of metal nitrate solution at a concentration of 0.5 mmol dm^{-3} with respect to the metal ion in a screw-capped polypropylene bottle at 25 ℃. After 24 h, the supernatant liquors were recovered by centrifugation at 1500 g for 5 min and analysed by inductively coupled plasma spectroscopy (ICP) using a TJA Iris simultaneous ICP-OES spectrophotometer. Each experiment was carried out in triplicate.

3. Results and discussion

3.1 Characterisation of feldspathoid products

Powder XRD patterns of the ground amber container glass (ACG) and feldspathoid products prepared in 4 M $NaOH_{(aq)}$ at 100 °C for 1, 3 and 10 days (*viz.* N-1, N-3 and N-10, respectively) are shown in Fig. 1. The compositions of the feldspathoid products and identifying powder diffraction file (PDF) numbers of the principal hydroxysodalite and hydroxycancrinite ($Na_4(AlSiO_4)_3(OH).H_2O$) phases and the secondary katoite ($Ca_3Al_2(SiO_4)(OH)_8$) and tobermorite ($Ca_5Si_6O_{16}(OH)_2.4H_2O$) phases are listed in Table 2. XRD analysis demonstrates that, within 1 day under the selected reaction conditions, approximately 48% of the amorphous glass phase is transformed into crystalline products (Table 2, Fig.2). The rate of development of the crystalline phases subsequently slows such that the extents of conversion of the glass are 55 and 63% after 3 and 10 days, respectively; and a modest increase in the yield of solid product from 4.9 to 5.6 g is observed between 1 and 10 days.

Feldspathoid minerals are thermodynamically metastable phases whose formation obeys the Ostwald Law of Successive Transformations under hydrothermal conditions [26]. They are precipitated from solid parent materials in alkaline media by a dissolution, nucleation and growth mechanism during which a series of transitory intermediate phases is formed over time. In this study, the initial major product is hydroxysodalite, a proportion of which subsequently converts to hydroxycancrinite as the phase assemblage evolves (Fig. 2, Table 2). Similarly, previous research also reports the sequential transformation of sodalite to cancrinite during the hydrothermal treatment of kaolinite-rich clay in alkaline media and as by-products in the Bayer process [16,17].
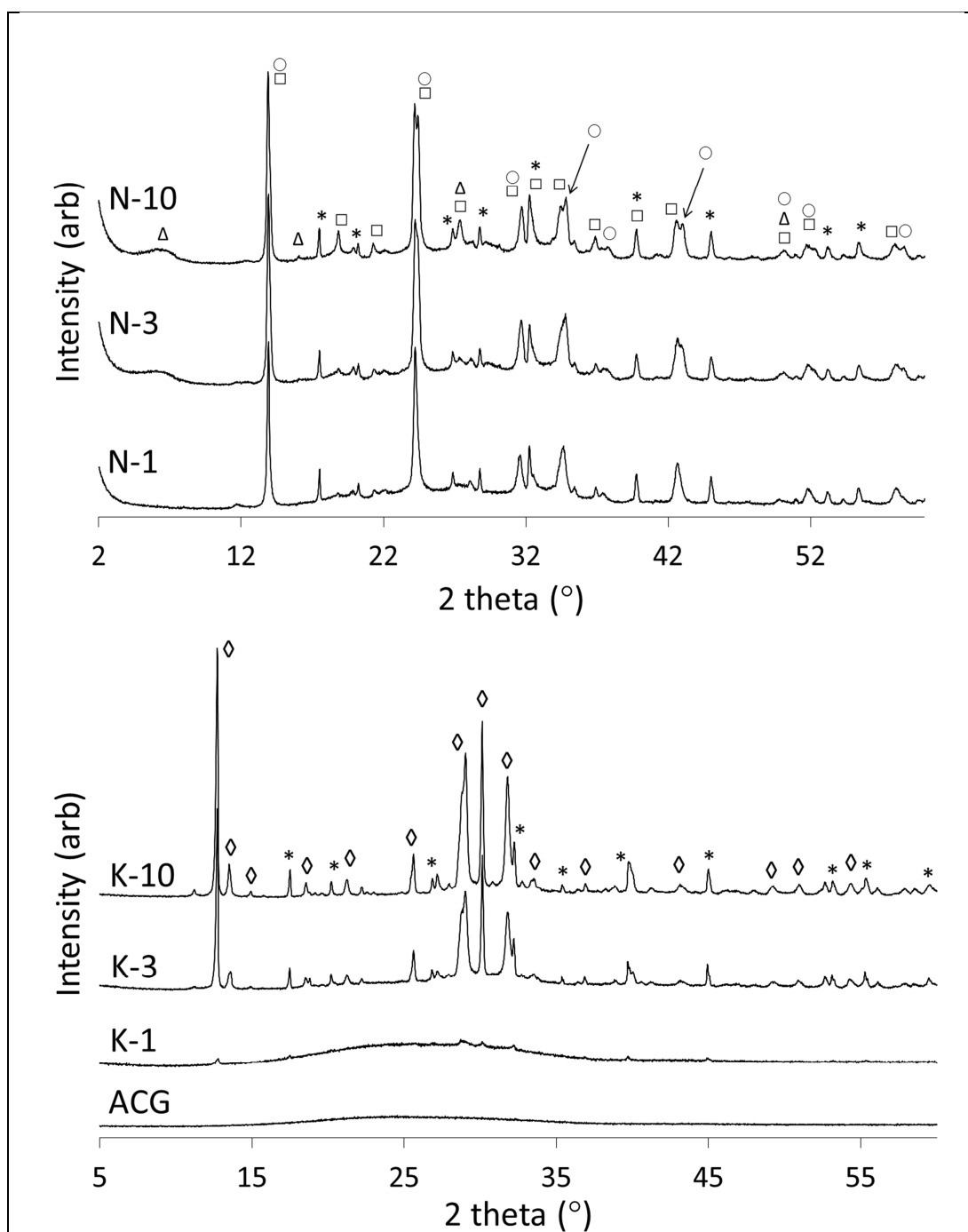
9

Fig. 1. XRD patters of waste amber container glass (ACG) and hydrothermal products synthesised for 1, 3 and 10 days in $NaOH_{(aq)}$ (*viz*. N-1, N-3, N-10) and $KOH_{(aq)}$ (*viz*. K-1, K-3, K-10) at 100 °C. Key: ◊ - zeolite K-F; * - katoite; ○ - hydroxysodalite; □ - hydroxycancrinite; Δ - tobermorite.

The hydrogarnet, katoite, is consistently present among the reaction products at approximately 6 wt% throughout the hydrothermal treatment of the amber glass, and the layer-lattice inosilicate phase, tobermorite, also develops as the reaction proceeds (Fig. 2, Table 2). These calcium aluminosilicate phases arise from a stoichiometric excess of calcium in the glass feedstock with respect to the maximum possible substitution of Ca^{2+} for Na^+ in the feldspathoid phases.

Table 2. Compositions and surface areas of hydrothermal feldspar and zeolite K-F products.

| Phase	N-1	N-3	N-10
Hydroxysodalite (PDF 073-5303) (wt%)	29.19 ± 1.25	25.71 ± 0.52	26.15 ± 2.62
Hydroxycancrinite (PDF 046-1457) (wt%)	11.22 ± 0.98	14.37 ± 0.73	19.58 ± 1.77
Katoite (PDF 077-1713) (wt%)	6.65 ± 0.39	5.58 ± 0.22	6.16 ± 0.03
Tobermorite (PDF 006-0005) (wt%)	0.43 ± 0.40	9.63 ± 1.97	10.69 ± 1.17
Weighted profile R-factor (R_{wp})	7.7	8.0	8.9
Goodness of fit (GOF)	2.5	2.6	3.0
Crystallinity (%)	47.5 ± 3.0	55.4 ± 1.9	62.6 ± 1.8
Yield (g)	4.92 ± 0.09	5.37 ± 0.07	5.57 ± 0.03
Specific surface area ($m^2\ g^{-1}$)	1.59 ± 0.15	2.01 ± 0.05	3.26 ± 0.03
Phase	**K-1**	**K-3**	**K-10**
Zeolite K-F (PDF 025-0619) (wt%)	3.71 ± 0.33	49.39 ± 0.09	63.61 ± 0.13
Katoite (PDF 084-0917) (wt%)	1.69 ± 0.33	10.96 ± 0.09	14.34 ± 0.13
Weighted profile R-factor (R_{wp})	3.2	10.3	14.3
Goodness of fit (GOF)	1.0	2.9	4.0
Crystallinity (%)	5.4 ± 0.3	60.4 ± 0.4	78.0 ± 0.6
Yield (g)	2.09 ± 0.18	4.01 ± 0.11	6.45 ± 0.02
Specific surface area ($m^2\ g^{-1}$)	2.70 ± 0.02	1.49 ± 0.03	1.84 ± 0.09
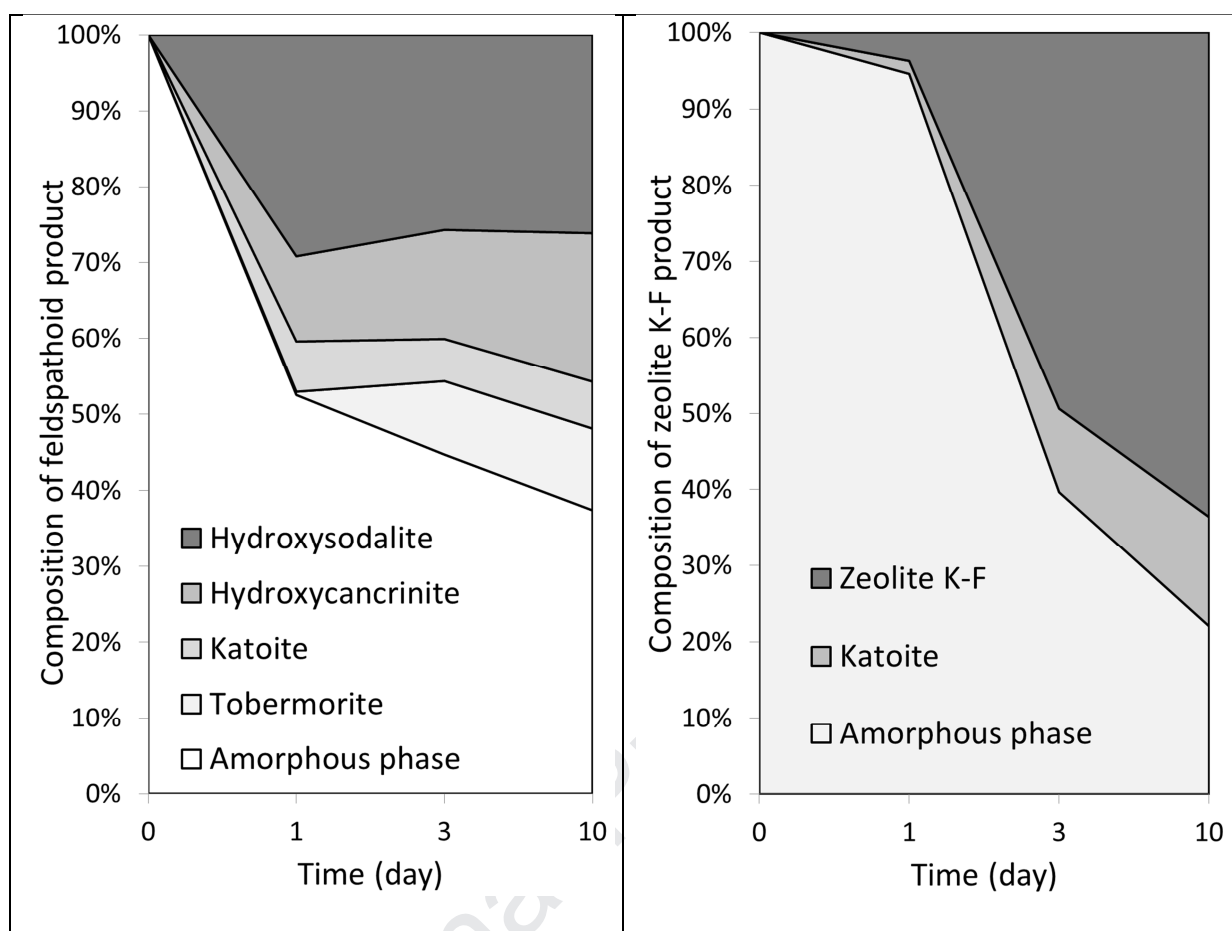
Fig. 2. Phase compositions of the hydrothermal feldspathoid and zeolite K-F products synthesised for 1, 3 and 10 days in NaOH$_{(aq)}$ and KOH$_{(aq)}$, respectively.

FTIR spectra of the amber container glass and feldspathoid products are given in Fig. 3. The spectrum of the amber glass comprises a broad medium intensity signal at 775 cm^{-1} which is assigned to symmetrical Si-O-Si stretching vibrations and a very broad strong asymmetrical combination band centred around 1000 cm^{-1} arising from antisymmetric stretching of the polymerised Si-O-Si system and non-bridging Si-O^{-} groups within the amorphous silicate network of the glass [27].
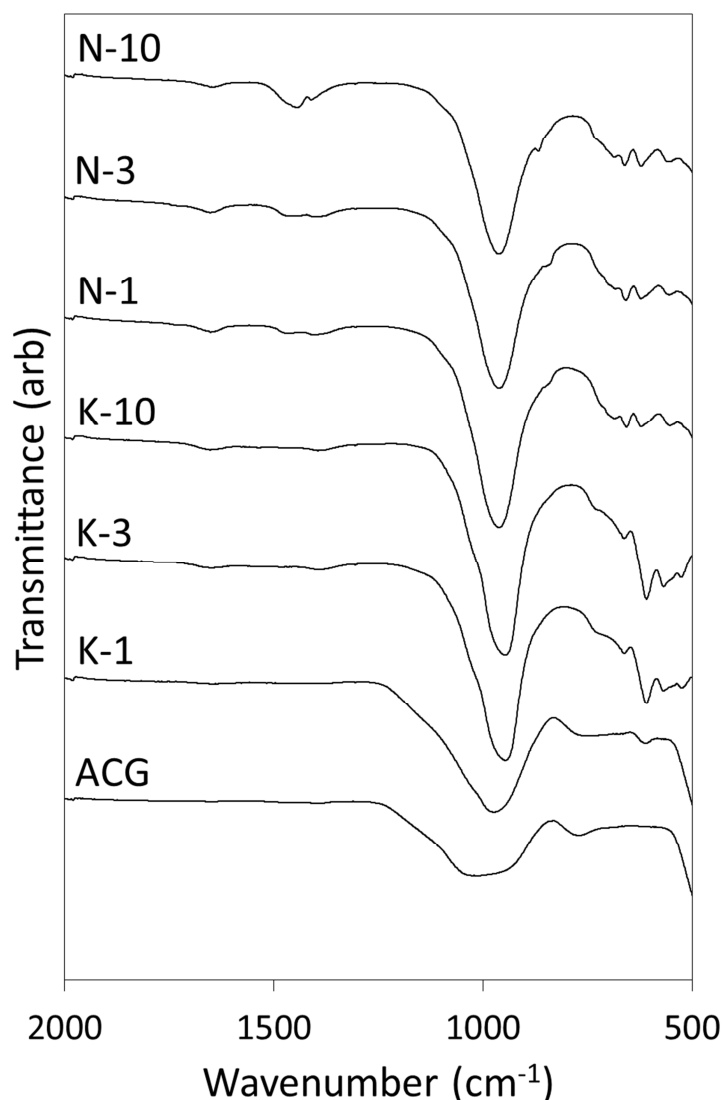
12

Fig. 3. FTIR spectra of amber container glass (ACG) and hydrothermal products synthesised

for 1, 3 and 10 days in NaOH$_{(aq)}$ (*viz*. N-1, N-3, N-10) and KOH$_{(aq)}$ (*viz*. K-1, K-3, K-10).

The FTIR spectra of the feldspathoid products (Fig. 3) exhibit characteristic vibrations

of the aluminosilicate frameworks of hydroxysodalite and hydroxycancrinite [16,28].

Antisymmetric stretching of the Si(Al)-O-Si frameworks gives rise to an intense broad

combination band *circa* 960 cm^{-1} [16,28]. The narrowing of this main antisymmetric

framework stretching band observed for the feldspar products relative to that of the amber

glass denotes the increasing structural organisation within the hydroxysodalite and

hydroxycancrinite lattices in comparison with the amorphous nature of the parent material.

13

Weaker, poorly resolved bands at 687, 661, 624 and 555 cm^{-1} are assigned to various characteristic O-Si(Al)-O bending modes and the shoulder at 725 cm^{-1} is attributed to symmetrical stretching vibrations of the feldspathoid lattices [16,28]. Scissor bending vibrations of adsorbed molecular water and hydroxyl groups appear at approximately 1645 cm^{-1} and calcite gives rise to bands at 1450 and 870 cm^{-1} which intensify with reaction time. Calcite commonly forms by atmospheric carbonation of calcium-bearing materials under alkaline conditions. In this case, calcite is not evident in the corresponding XRD patterns (Fig. 1) which indicates that it is too poorly crystalline and/or not in sufficient abundance to be detected by this technique. Discrete signals arising from katoite and tobermorite are not apparent in the FTIR spectra of the feldspathoid products as these are obscured by the various lattice vibrations of the principal hydroxysodalite and hydroxycancrinite phases (Fig. 3).

The ^{29}Si MAS NMR spectra of the ground amber container glass and feldspathoid product after hydrothermal synthesis for 10 days (N-10) are shown in Fig. 4. The spectrum of the parent amber glass displays a very broad asymmetrical signal with maximum intensity at approximately -94 ppm which is consistent with a range of amorphous Q^2-Q^4 silicate units comprising a predominance of Q^3 species. This spectrum closely resembles those reported in the literature for soda-lime-silica container glass of similar composition [29,30].

The ^{29}Si MAS NMR spectrum of the 10-day feldspathoid product comprises an asymmetrical signal at -88 ppm principally arising from the Q^4(4Al) sites in hydroxysodalite and hydroxycancrinite [31,32]. This is in agreement with the expected chemical shift for a 1:1 ratio of alternating SiO_4 and AlO_4 units within a framework lattice [31,32]. It should be noted that the framework structures of feldspathoids are governed by Lowenstein's rule which forbids the formation of direct Al-O-Al bonds and limits the maximum possible Al:Si ratio to unity.
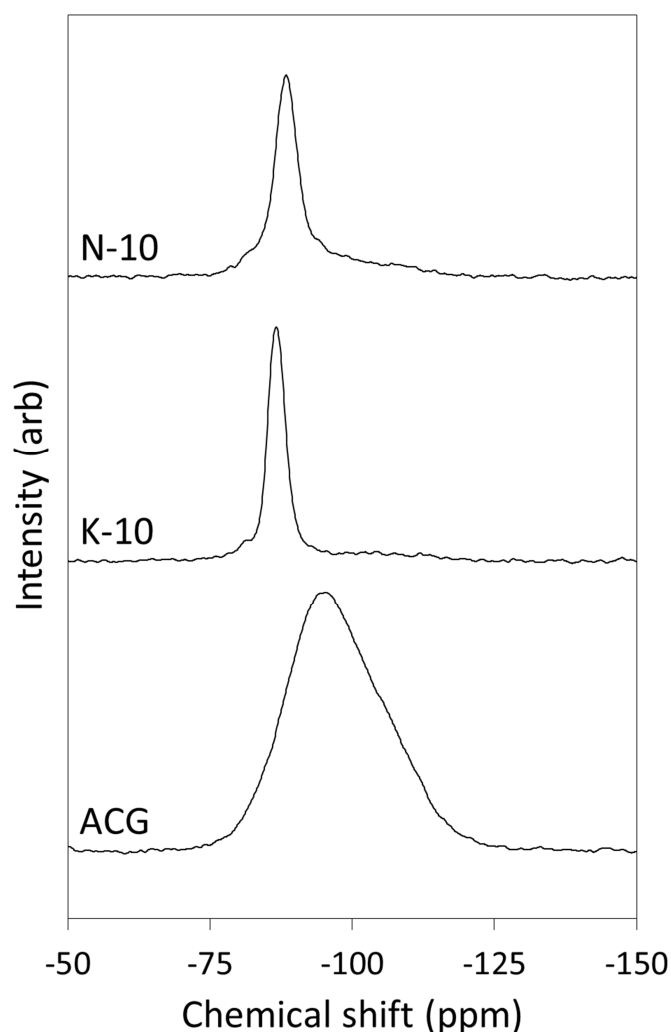
14

Fig. 4. ^{29}Si MAS NMR spectra of amber container glass (ACG) and hydrothermal products synthesised for 10 days in NaOH$_{(aq)}$ (N-10) and KOH$_{(aq)}$ (K-10), respectively.

The principal Q^4(4Al) resonance from the feldspathoids (Fig. 4) is superposed over a weaker very broad signal arising from residual parent glass and possibly also from an amorphous geopolymeric aluminosilicate gel phase that may have formed during hydrothermal processing [15]. The upfield shoulder at -80 ppm is assigned to the silicate centres in katoite that are linked with four octahedrally coordinated aluminate units [33]; and signals arising from the Q^2, Q^2(1Al) and Q^3 species of tobermorite are obscured by the resonances of the feldspathoid and amorphous phases. In this instance, no spectral

15

deconvolution was attempted owing to the poor definition of the signal arising from the amorphous material and the inability to accurately predict the positions and relative intensities of the individual signals of the poorly crystalline tobermorite phase.
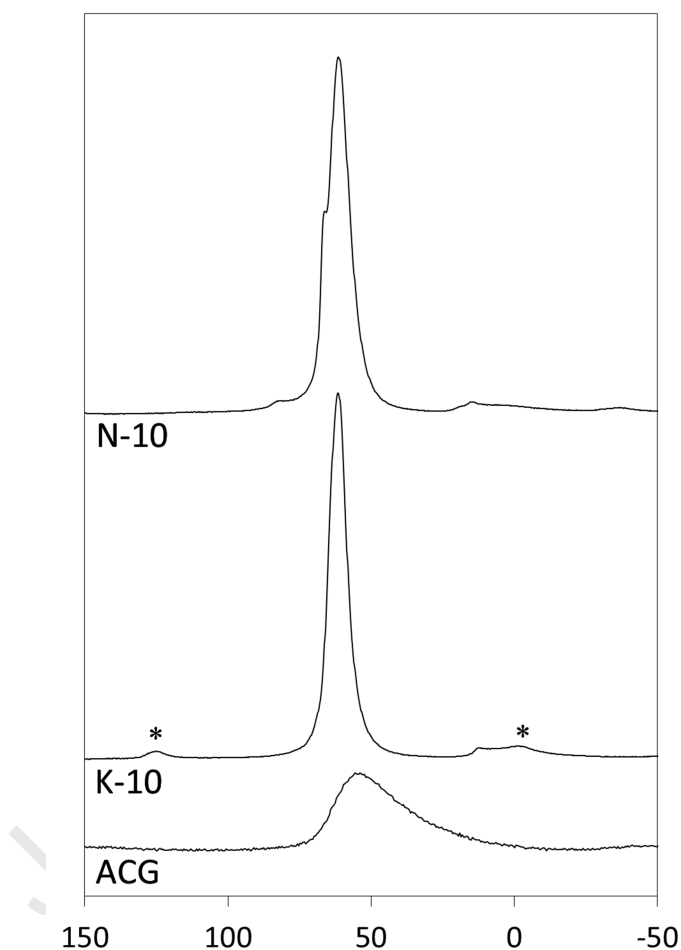

Fig. 5. ^{27}Al MAS NMR spectra of amber container glass (ACG) and hydrothermal products synthesised for 10 days in NaOH$_{(aq)}$ (N-10) and KOH$_{(aq)}$ (K-10), respectively.

^{27}Al MAS NMR spectroscopy is used to discriminate among different aluminium coordination environments in inorganic solids [34]. Tetrahedrally coordinated aluminium units give rise to signals in the approximate chemical shift range of 100 to 50 ppm; and octahedral aluminium resonates between 20 and -10 ppm [34]. The ^{27}Al MAS NMR spectrum

of the amber container glass is shown in Fig. 5 and comprises one very broad resonance of maximum intensity at ~54 ppm that is assigned to the highly disordered tetrahedral aluminium species within the amorphous glass network. The tetrahedral aluminium environments of the feldspathoid phases of the 10-day hydrothermal product, N-10, give rise to the asymmetrical signal centred at 61.9 ppm (Fig. 5) [31,32]; and the shoulder at 66.5 ppm is attributed to AlO_4^{5-} units substituted into the silicate chains of tobermorite [35]. The presence of katoite is denoted by the octahedral aluminate resonance at 13.5 ppm [33].

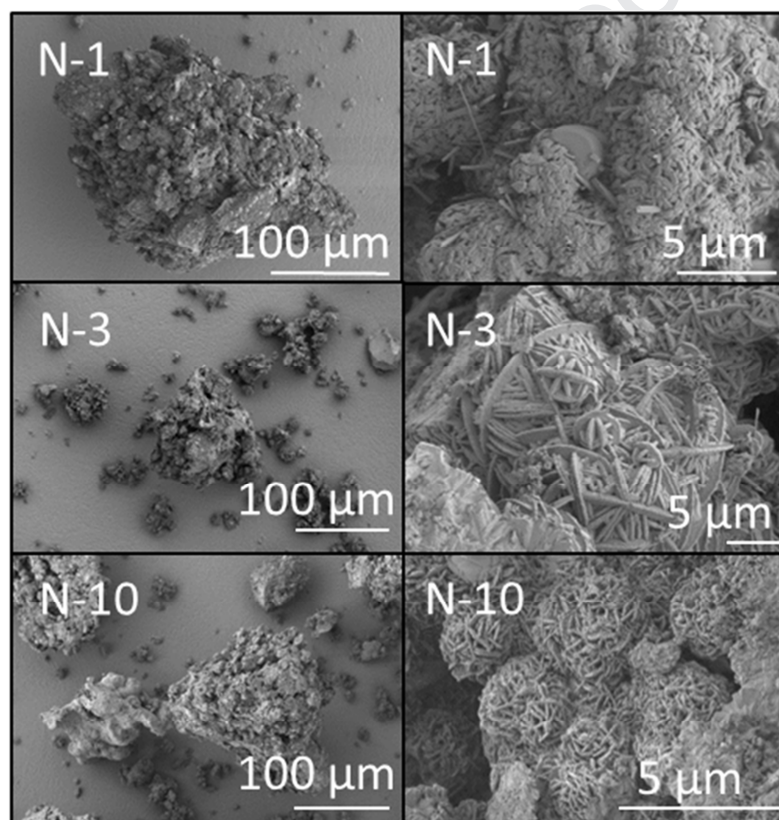**Fig. 6.** Secondary electron SEM images of hydrothermal feldspathoid products synthesised for 1, 3 and 10 days in $NaOH_{(aq)}$ (*viz.* N-1, N-3 and N-10, respectively)

Scanning electron microscopy (Fig. 6) indicated that the feldspathoid products are granular materials with the majority of particles in the size range 50 - 300 μm. The surfaces

of the particles are populated with the characteristic bevelled ball-of-wool morphologies of hydroxysodalite which are interspersed with lath-like crystals of hydroxycancrinite (Fig. 6). Globular, botryoidal deposits also feature on the surface of the 1-day samples which disappear within 3 days and are a considered to be an early aluminosilicate gel precursor to the hydroxysodalite phase. Additional SEM images are provided in the supplementary information to further illustrate the morphologies of the hydration products. The BET external surface area of the ground amber glass was initially below 0.5 m^2 g^{-1} (*i.e.* below the measurement limit of the instrument) and steadily increased to 3.3 m^2 g^{-1} after 10 days of hydrothermal processing in sodium hydroxide solution (Table 2). It should be noted that, the BET surface area measurements made in this study refer exclusively to the external surfaces of the samples. Under the selected degassing and analysis conditions, retained water and the failure of nitrogen to effectively penetrate the ultramicropores of the feldspathoids prevent the measurement of the internal surface area and porosity [36].

The molar elemental compositions of the feldspathoid products were determined by EDX analysis and are listed in Table 3. The initial Al:Si ratio of the parent amber glass, determined by XRF to be 1:27 (Table 1), is seen to increase dramatically to 1:0.87 (Table 3) within 1 day of hydrothermal processing which demonstrates considerable dissolution of the glass and formation of the more Al-rich products. Equimolar quantities of Al and Si were initially present in the reaction mixture, yet the Al:Si ratio of the products is consistently greater than unity at all times indicating that a significant proportion of silicate species are partitioned in the reaction liquor. Similarly, an increase in initial Na:Si ratio of the amber glass from 1:2.7 (Table 1) to 1:0.79 in the 1-day hydrothermal product is also indicative of the extensive dissolution of the glass and precipitation of the more Na-rich product phases. The trace element constituents of the amber glass, potassium, iron, sulphur and chromium,

were not detected by EDX analysis in any of the hydrothermal reaction products indicating that they are present below 0.01 mol% if at all.

Table 3. Molar elemental compositions of feldspathoid and zeolite K-F hydrothermal products synthesised for 1, 3 and 10 days in $NaOH_{(aq)}$ and in $KOH_{(aq)}$. Standard deviations of the mean values are given in brackets.

Sample	Si (mol%)	Al (mol%)	K (mol%)	Ca (mol%)	Na (mol%)	Mg (mol%)	C (mol%)	O (mol%)
N-1	7.30 (0.33)	8.37 (0.38)	below detection	1.13 (0.15)	9.30 (0.67)	0.32 (0.15)	2.15 (0.23)	71.45 (0.64)
N-3	8.12 (0.38)	8.58 (0.56)	below detection	0.73 (0.19)	8.88 (0.19)	0.22 (0.08)	1.85 (0.30)	72.10 (1.10)
N-10	6.83 (0.74)	7.85 (0.67)	below detection	1.13 (0.21)	10.63 (0.76)	0.25 (0.14)	2.40 (0.54)	70.95 (0.81)
K-1	14.78 (0.93)	3.08 (1.68)	1.83 (1.16)	2.83 (0.57)	3.88 (0.80)	0.53 (0.08)	2.52 (0.23)	70.45 (2.13)
K-3	9.88 (0.81)	9.00 (1.31)	8.46 (1.99)	1.52 (0.32)	0.90 (0.51)	0.38 (0.08)	2.74 (0.56)	67.18 (2.62)
K10	8.28 (0.33)	9.22 (0.37)	10.28 (1.13)	0.85 (0.27)	0.50 (0.06)	0.27 (0.10)	3.03 (0.24)	67.62 (1.46)

The observed increase in the molar oxygen content of the hydrothermal feldspathoid products (>70 mol%) relative to that of the amber glass (~60 mol%) is attributed to the presence of water and hydroxyl ions in the products (since hydrogen atoms are not detected by EDX analysis). Carbon is present within the feldspathoid products in the form of trace quantities of calcite; although, it should be noted that carbon is overrepresented in the EDX analyses of these samples owing to the contribution from the carbon tabs on which they were mounted.

3.2 Characterisation of zeolite K-F products

Powder XRD patterns of the zeolite K-F products prepared in 4 M $KOH_{(aq)}$ at 100 °C for 1, 3 and 10 days (respectively, K-1, K-3 and K-10) are compared with that of the parent amber glass in Fig. 1. The compositions of the zeolite K-F products are listed in Table 2 and the evolution of the phase assemblage is plotted in Fig. 2. Under the selected reaction conditions, the initial development of the two product phases, zeolite K-F and katoite, is slow with only ~5% crystallinity having been achieved within the first 24 h. The reaction rate then markedly increases to give a product of ~60% crystallinity at 3 days and subsequently slows again such that the final 10-day product is 78% crystalline. The total yield of solid product increases from 2.1 g to 6.5 g between 1 and 10 days.

Other researchers have also observed that the initial crystallisation of K-zeolites from paper sludge ash and coal fly ash is slower than that of Na-zeolites [37]. In comparison with the abundant research undertaken to synthesise Na-zeolites from various waste materials in $NaOH_{(aq)}$, literature on the production of K-zeolites is relatively sparse with only one report, to date, describing the hydrothermal processing of soda-lime-silica glass in $KOH_{(aq)}$ [15]. In this study, Terzano *et al*. [15] report that 25 wt% zeolite K-F and a minor unidentified phase were produced from a mixture of 8 g of flint container glass and 0.5 g of aluminium alloy (from soda cans) in 80 cm^3 of 5 M $KOH_{(aq)}$ at 90 °C for 7 days [15]. The superior yield of zeolite K-F (49 wt% at 3 days) observed in the present study was obtained by increasing the Al:Si ratio of the reaction composition to unity and by raising the temperature by 10 °C.

Previous studies on the hydrothermal processing of K-feldspar-CaO-KOH-H_2O mixtures have demonstrated that the stability of zeolite K-F is favoured above 95 °C at $KOH_{(aq)}$ concentrations in the range 4 - 5 M, and that a wide range of additional temperature-dependent calcium aluminosilicate phases arise if calcium ions are present in stoichiometric

excess [20,38]. Since zeolite K-F can accommodate little to no calcium ions during formation, in the present study, an Al:Si ratio of 1:1 was selected rather than the target 2:3 stoichiometric Al:Si ratio of zeolite K-F in order to provide additional aluminium for reaction with 'unwanted' calcium ions from the parent glass to form katoite. Under the selected reaction conditions, the results indicate that after the initial slow dissolution of the glass and low yield of products within the first 24 h, the concomitant precipitation of katoite helps to drive the formation of zeolite K-F which significantly improves the yield at 3 and 10 days.

FTIR spectra of the zeolite K-F products are compared with that of the amber container glass in Fig. 3. The very broad band of the antisymmetric stretching of the Si-O-Si network in the glass persists in the spectrum of the 1-day product over which is superimposed a sharper signal from the O-Si(Al)-O stretching vibrations of the zeolite K-F lattice with maximum intensity at ~985 cm^{-1} [21,27]. The medium broad band arising from symmetrical Si-O-Si stretching vibrations of the glass is also present in this spectrum at 775 cm^{-1} and a broad signal appears at 610 cm^{-1} from the zig-zag modes of the 8-membered ring subunits of zeolite K-F [27]. As the reaction proceeds, the antisymmetric stretching of the Si-O-Si polymer system of the glass is successively replaced by the lattice stretching of zeolite K-F which is centred at 965 cm^{-1}. Symmetrical Si-O-Al lattice vibrations develop at 665 cm^{-1} and the zig-zagging of the 8-membered rings subsequently differentiates into two individual bands at 610 and 570 cm^{-1} [21]. A framework O-Si(Al)-O bending mode also gives rise to a signal at 527 cm^{-1}. Discrete signals arising from katoite are not observed in the FTIR spectra as they are obscured by the various vibrational modes of the zeolite K-F lattice. Broad low intensity signals of the stretching and bending modes of water and hydroxyl groups at 1648 cm^{-1} are present in the spectra of all of the hydrothermal zeolite K-F products.

The formation of the principal crystalline zeolite K-F phase is confirmed by the symmetrical Q^4(4Al) resonance at ~-86 ppm in the ^{29}Si MAS NMR spectrum of the 10-day

product (Fig. 4) [39]; and the poorly resolved upfield shoulder at ~-81 ppm arises from the silicate centres in the minor katoite phase [33]. Likewise, the resonance at 61.8 ppm in the ^{27}Al MAS NMR spectrum of the 10-day product (Fig. 5) is characteristic of the tetrahedral aluminium environment in zeolite K-F [39] and the signal at 13.9 ppm is assigned to the octahedrally coordinated aluminium centres in katoite [33].

Scanning electron microscopy indicated that the zeolite K-F products principally consist of bimodally distributed granular particles in the approximate size ranges 5 - 10 μm and 50 - 200 μm (Fig. 7); the former arising from nucleation and growth in solution, and the latter by direct precipitation and growth on the surface of the parent glass particles.
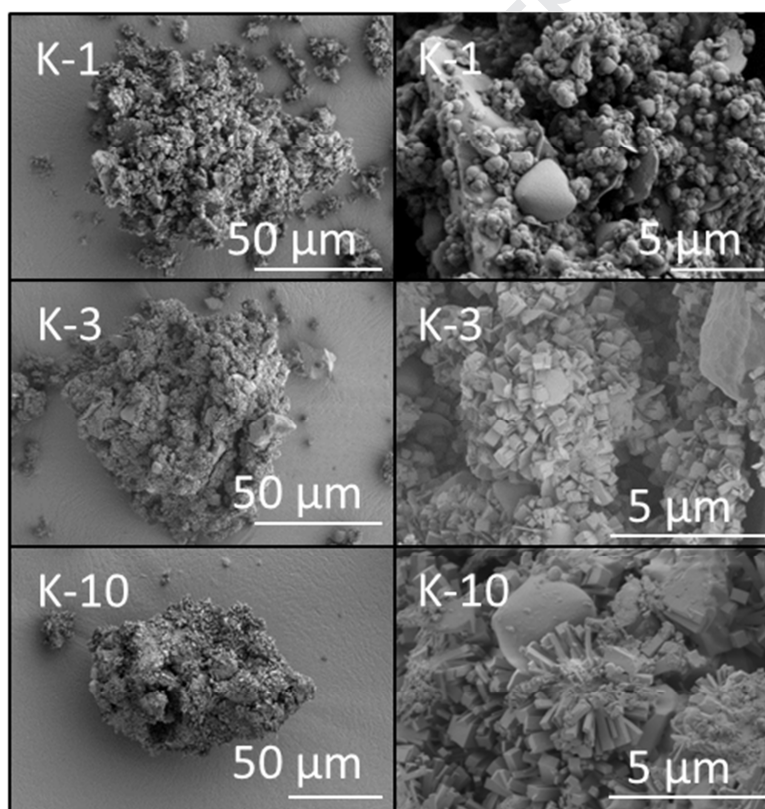

Fig. 7. Secondary electron SEM images of hydrothermal zeolite K-F products synthesised for 1, 3 and 10 days in KOH$_{(aq)}$ (*viz.* K-1, K-3 and K-10, respectively)

Initial 1-day hydration products appear as textured distorted spherical bundles which are distributed across, but do not wholly cover, the surface of the glass. Similar aggregated spherical bundles are also found as discrete <10 μm grains. These poorly defined spheres are thought to be an aluminosilicate gel precursor to the zeolite K-F phase. Within 3 days, sub-micron tetragonal crystals of zeolite K-F are seen to entirely populate the surfaces of the grains among which are dispersed occasional hexagonal plates of katoite and some remaining distorted spheres. As the reaction progresses, crystalline products incompletely fill the lacunae created by the continuing dissolution of the glass to produce porous hierarchical structures and the tetragonal zeolite K-F crystals continue to grow to between 2 and 5 μm in length by 10 days. More detailed SEM micrographs of the zeolite K-F hydration products are provided in the supplementary information.

The BET surface area of the zeolite K-F products initially increases from below the measurable limit of 0.5 m^2 g^{-1} for the ground parent glass to 2.7 m^2 g^{-1} within 1 day, as the first hydration products appear (Table 2). The surface area then decreases by 3 days (to ~1.5 m^2 g^{-1}) as the zeolite K-F and katoite phases develop and subsequently increases again with the ongoing dissolution of the glass and growth of the crystalline products (to ~1.8 m^2 g^{-1} at 10 days). As previously mentioned, in this case, only the external surface area is expressed in these measurements as nitrogen molecules are unable to probe the interior of the zeolite K-F micropores without undertaking bespoke degassing and adsorption-desorption regimes [36].

The molar elemental compositions of the zeolite K-F products are listed in Table 3. The partial dissolution of the parent glass and formation of the early hydration products after 1 day are demonstrated by the concomitant increases in the molar ratios of Al:Si (from 1:27 to 1:4.8) and K:Si (from 1:65 to 1:8.1) (Tables 1 and 3). These ratios subsequently increase further at 3 and 10 days, as the dissolution of the glass continues and the zeolite K-F and katoite phases develop. Likewise, the successive reduction in Na:(Si+Al) ratio from 1:2.8 for

the initial glass to 1:35 after 10 days is also associated with the conversion of the glass into the crystalline products that do not favour the accommodation of sodium ions. However, residual sodium ions are likely to persist in the amorphous aluminosilicate gel phase observed by SEM (Fig. 7) and also in any remaining unreacted glass.

3.3 Uptake of Pb^{2+} and Zn^{2+} ions by the feldspathoid and zeolite K-F products

Divalent lead and zinc ions are among the most commonly occurring heavy metals in industrial wastewater and have accordingly been selected as model contaminants to evaluate the sorptive properties of the feldspathoid and zeolite K-F products [40]. The uptakes of Pb^{2+} and Zn^{2+} ions by the 10-day feldspathoid and zeolite K-F products from single metal ion solutions during batch sorption are compared with those of other waste-derived inorganic sorbents in Table 4 [11,41-49]. Natural, synthetic and waste-derived zeolites commonly exhibit cation exchange capacities (CECs) between 1 and 5 meq g^{-1} [15,50], and in the present study the observed uptakes of Pb^{2+} (4.3 and 4.5 meq g^{-1} for N-10 and K-10, respectively) and Zn^{2+} (3.9 and 4.1 meq g^{-1} for N-10 and K-10, respectively) fall within the expected range. Despite the incomplete conversion of amber glass into zeolitic phases, the uptake capacities of the N-10 and K-10 products for Pb^{2+} and Zn^{2+} ions appear towards the top end of the anticipated CEC range for zeolites and are generally greater than those of many other waste-derived inorganic sorbents reported in the literature (Table 4) [11,41-50]. The superior sorption capacities are attributed to the high Al:Si ratios of the feldspathoid and zeolite K-F phases which confer the aluminosilicate frameworks with increased anionic charge, polarity and hydrophilicity [50]. The greater sorption capacity of the feldspathoid and zeolite K-F products for Pb^{2+} over Zn^{2+} is attributed to the smaller hydrated radius of former ion (0.401 nm for Pb^{2+} and 0.430 nm for Zn^{2+}). This phenomenon has similarly been

observed in other studies where cations with smaller hydrated radii are absorbed more rapidly

and in greater quantity by microporous low-silica zeolites [51-53].

Table 4. Uptakes of Pb^{2+} and Zn^{2+} by hydrothermal reaction products N-10 and K-10

and by other waste-derived inorganic sorbents

Sample	Pb^{2+}-uptake (mmol g^{-1})	Pb^{2+}-uptake (mg g^{-1})	Zn^{2+}-uptake (mmol g^{-1})	Zn^{2+}-uptake (mg g^{-1})	Ref.
N-10	2.17 ± 0.80	450 ± 166	1.95 ± 0.10	128 ± 7	-
K-10	2.27 ± 0.72	470 ± 149	2.06 ± 0.10	135 ± 7	-
Rice husk ash	-	129	-	-	[41]
Blast furnace sludge	-	79.87	-	9.25	[42]
Red mud	-	64.79	-	12.59	[43]
Concrete fines	-	37	-	33	[44]
Zeolite NaP1 (fly ash)	-	266.4	-		[45]
Zeolite NaP1 (fly ash)	-		-	94.4	[46]
Sodalite (fly ash)	-	157.2	-	-	[47]
Cancrinite (fly ash)	2.530	-	1.154	-	[48]
Tobermorite	-	467	-	-	[11]
Geopolymer (fly ash)	-	166.55	-	-	[49]

General applications of the low-silica zeolites include the removal of metal ions from

aqueous waste streams, and in this respect, the container glass-derived feldspathoids are

attractive candidate sorbents owing to their competitive CECs. Zeolite K-F synthesised from

the hydrothermal treatment of K-feldspar is currently proposed as an alternative slow-release

agricultural fertiliser to address the predicted shortage in potash [20,38]. The concomitant

release of K^+ ions and uptake of toxic metal ions such as Pb^{2+} indicates that zeolite K-F may

also find application in soil remediation processes.

3.4 Waste container glass for the synthesis of feldspathoid and zeolite phases

For the past three decades, increasing efforts have been made to prepare zeolites and other technologically significant silicate minerals from a wide range of high-volume industrial, agricultural and municipal waste streams [4,6-15,18,21-23,30,37,39,41-49,54,55]. The current global market for synthetic zeolites is estimated to be 5.2 billion USD *per annum* [55] and the potential use of waste materials represents significant reductions in energy, natural resources, cost, waste disposal and unwanted emissions.

A current SWOT analysis to determine the *Strengths*, *Weaknesses*, *Opportunities*, and *Threats* of producing zeolite A from waste resources, highlights the need to develop 'one-pot' synthesis strategies as multi-stage processes are time-consuming and costly [55]. In this respect, container glass is an attractive feedstock for the one-pot hydrothermal synthesis of zeolites, as additional pre-conditioning and processing stages are optional, rather than necessary, and could be implemented on a value-added basis.

To date, simple one-pot hydrothermal methods have been used to prepare various mixtures of sodalite, cancrinite, analcime, zeolite X, zeolite NaP1 and zeolite A from ground container glass combined with numerous aluminium sources in sodium hydroxide solution [6-9,15,56-58]. Under these conditions, the presence of 5-10 wt% of CaO in the glass limits the development of framework silicate phases that do not tolerate the incorporation of Ca^{2+} ions during formation [6]. This tends to favour the small pore feldspathoid zeolites (*e.g.* sodalite, cancrinite and analcime) that can readily accommodate charge-balancing labile Ca^{2+} ions during crystallisation, and also gives rise to other minor hydrated calcium aluminosilicate phases such as tobermorite and katoite, as has been observed in the present study [6,7,15].

As previously mentioned, reports of the direct synthesis of zeolites from fine chemical reagents and waste materials in $KOH_{(aq)}$ [18-23] are considerably fewer in number than those of Na-zeolites, with only one study on the hydrothermal conditioning of container glass in $KOH_{(aq)}$ [15]. Nonetheless, the kinetics of zeolitisation of paper sludge ash and coal fly ash in $KOH_{(aq)}$ are unanimously reported to be slower than those in $NaOH_{(aq)}$ with respect to both the dissolution of the parent glassy phases and also the nucleation and growth of the products [23,36,59]. The findings of the present study similarly indicate that the dissolution of the soda-lime-silica glass and the initial precipitation of the zeolite product in $KOH_{(aq)}$ are considerably slower than those observed in $NaOH_{(aq)}$. However, after 1 day, the subsequent development of zeolite K-F was greater than that of the feldspathoids and ultimately resulted in products of higher yield and crystallinity within 3 and 10 days (Table 2, Fig. 2).

One potential strategy to improve the kinetics and yield of zeolite K-F from container glass may be to employ a reaction medium comprising a two-component mixture of alkali metal hydroxides rather than pure $KOH_{(aq)}$. Previously, using this approach, Wajima and Munaka [23] were able to enhance the formation of zeolite K-F from paper sludge ash in a binary solution of 3 M $KOH_{(aq)}$ and 1M $LiOH_{(aq)}$ rather than in 4 M $KOH_{(aq)}$ alone. Microwave synthesis is also a promising option for the rapid zeolitisation of container glass. Majdinasab *et al*. [8] have recently demonstrated that microwave synthesis can be used to drastically reduce reaction time for the synthesis of various zeolite mixtures from pulverised container glass and sodium aluminate in $NaOH_{(aq)}$. Similarly, the rapid microwave synthesis of zeolite K-F from rice husk ash has been documented [21] and this technique may also be applicable to the efficient synthesis of this zeolite from waste container glass.

27

4. Conclusions

This study has confirmed that feldspathoids (hydroxysodalite and hydroxycancrinite) and zeolite K-F can be prepared by one-pot hydrothermal synthesis from a mixture of amber container glass and aluminium waste (Al:Si = 1) at 100 °C in 4 M $NaOH_{(aq)}$ and 4 M $KOH_{(aq)}$, respectively. A mixture of hydroxysodalite (HS) and hydroxycancrinite (HC) with minor proportions of katoite and tobermorite formed in $NaOH_{(aq)}$ and the subsequent partial conversion of HS to HC was observed between 1 and 10 days. The initial rates of dissolution of the glass and precipitation of the major zeolite K-F and minor katoite phases were considerably slower in $KOH_{(aq)}$; although, within 10 days the crystallinity of the zeolite K-F sample (78%) was superior to that of the feldspathoid product (63%). Despite the incomplete conversion of amber glass into crystalline zeolitic phases, the uptake capacities of the 10-day feldspathoid and zeolite K-F products for Pb^{2+} and Zn^{2+} ions compared favourably with those of other waste-derived inorganic sorbents reported in the literature. Waste coloured container glass is a particularly attractive feedstock for the facile one-pot synthesis of feldspathoids and zeolites as, unlike many industrial silicate-bearing wastes, it does not require pre-treatment for activation or removal of hazardous components.

28

References

[1] R. Conradt, Prospects and physical limits of processes and technologies in glass melting, J. Asian Ceram. Soc. (2019) https://doi.org/10.1080/21870764.2019.1656360.

[2] R.C.G. Beerkens, New concepts for energy efficient and emission friendly melting of glass. Ceram. Trans. 231 (2012) 5-24.

[3] H. Gujba, A. Azapagic, Carbon footprint of beverage packaging in the United Kingdom, in: M. Finkbeiner (Ed.) Towards Life Cycle Sustainability Management, Springer, Dordrecht, 2011, pp. 381-390.

[4] N.J. Coleman, Q. Li, A. Raza, Synthesis, structure and performance of calcium silicate ion exchangers from recycled container glass, Physicochem. Probl. Miner. Process. 50 (2014) 5-16.

[5] M.F. Ashby, Materials and the Environment (Eco-informed Material Choice), second ed., Butterworth-Heinemann, Oxford, 2013.

[6] V.K. Elmes, B.N. Edgar, A.P. Mendham, N.J. Coleman, Basic metallosilicate catalysts from waste green container glass, Ceram. Int. 44 (2018) 17069-17073.

[7] A.R. Majdinasab, Q. Yuan, Microwave synthesis of zeolites from waste glass cullet using indirect fusion and direct hydrothermal methods: A comparative study, Ceram. Int. 45 (2019) 2400-2410.

[8] A.R. Majdinasab, P.K. Manna, Y. Wroczynskyj, J. van Lierop, N. Cicek, G.K. Tranmer, Q. Yuan, Cost-effective zeolite synthesis from waste glass cullet using energy efficient microwave radiation, Mater. Chem. Phys. 221 (2019) 272-287.

[9] A.R. Majdinasab, Q. Yuan, Microwave synthesis of zeolites from waste glass cullet using landfill leachate as a novel alternative solvent, Mater. Chem. Phys. 223 (2019) 613-622.

[10] R.V. Silva, J. de Brito, C.Q. Lye, R.K. Dhir, The role of glass waste in the production of ceramic-based products and other applications: A review, J. Clean. Prod. 167 (2017) 346-364.

[11] N.J. Coleman, C.J. Trice, J.W. Nicholson, 11 Å tobermorite from cement bypass dust and waste container glass: A feasibility study, Int. J. Miner. Process. 93 (2009) 73–78.

[12] N.J. Coleman, A.P. Hurt, A. Raza, Hydrothermal synthesis of lithium silicate (Li_2SiO_3) from waste glass: a preliminary study, Physicochem. Probl. Miner. Process. 51 (2015) 685-694.

[13] N. Marinoni, V. Diella, G. Confalonieri, A. Pavese, F. Francescon, Soda-lime-silica glass/quartz particle size and firing time: Their combined effect on sanitary-ware ceramic reactions and macroscopic properties, Ceram. Int. 43 (2017) 10895-10904.

[14] C. Bobiricǎ, J-H. Shim, J-Y. Park, Leaching behavior of fly ash-waste glass and fly ash-slag-waste glass-based geopolymers, Ceram. Int. 44 (2018) 5886-5893.

[15] R. Terzano, C. D'Alessandro, M. Spagnuola, M. Romagnoli, L. Medici, Facile zeolite synthesis from municipal glass and aluminium solid wastes, Clean-Soil Air Water 43 (2015) 133-140.

[16] C.A. Ríos Reyes, C. Williams, O.M.C. Alarcón, Nucleation and growth process of sodalite and cancrinite from kaolinite-rich clay under low-temperature hydrothermal conditions, Mater. Res. 16 (2013) 424-438.

[17] B. Xu, P. Smith, C. Wingate, L. De Silva, The effect of calcium and temperature on the transformation of sodalite to cancrinite in Bayer digestion, Hydrometallurgy 105 (2010) 75-81.

[18] V.S. Jakkula, C.D. Williams, T.J. Hocking, M.A. Fullen, High selectivity and affinity of Linde type F towards NH_4^+ on application as a soil amendment for maize growth, Microporous Mesoporous Mater. 88 (2006) 101-104.

[19] C. Belver, M.A. Vincente, Easy synthesis of K-F zeolite from kaolin, and characterization of this zeolite, J. Chem. Educ. 83 (2006) 1541-1542.

[20] J. Yuan, J. Yang, H. Ma, Q. Chang, Preparation of zeolite F as slow release fertilizers from K-feldspar powder, ChemistrySelect 2 (2017) 10722-10726.

[21] S.-F. Wong, K. Deekamwong, J. Wittakayun, T.C. Ling, O. Muraza, F. Adam, E.-P. Ng, Crystal growth study of K-F nanozeolite and its catalytic behaviour in Aldol condensation of benzanldehyde and heptanal enhanced by microwave heating, Mater. Chem. Phys. 196 (2017) 295-301.

[22] F. Miyaji, T. Murakami, Y. Suyama, Formation of Linde F zeolite by KOH treatment of coal fly ash, J. Ceram. Soc. Jpn. 117 (2009) 619-622.

[23] T. Wajima, K. Munakata, Effect of alkali species on synthesis of K-F zeolitic materials from paper sludge ash for soil amendment, Chem. Eng. J. 207-208 (2012) 906-912.

[24] A.A. Coelho, TOPAS and TOPAS-Academic: an optimization program integrating computer algebra and crystallographic objects written in C++, J. Appl. Cryst. 51 (2018) 210-218.

[25] N.J. Coleman, L.L. Hench, A gel-derived mesoporous silica reference material for surface analysis by gas sorption 1. Textural features, Ceram. Int. 26 (2000) 171-178.

[26] C.S. Cundy, P.A. Cox, The hydrothermal synthesis of zeolites: precursors, intermediates and reaction mechanism, Microporous Mesoporous Mater. 82 (2005) 1-78.

[27] H.A. El Batal, M.Y. Hassaan, M.A. Fanny, M.M. Ibrahim, Optical and FT infrared absorption spectra of soda lime silicate glasses containing nano Fe_2O_3 and effects of gamma irradiation, Silicon 9 (2017) 511-517.

[28] J. Yuan, J. Yang, H. Ma, C. Liu, C. Zhao, Hydrothermal synthesis of analcime and hydroxycancrinite from K-feldspar in Na_2SiO_3 solution: characterization and reaction mechanism, RSC Advances 6 (2016) 54503-54509.

[29] A.R. Jones, R. Winter, G.N. Greaves, I.H. Smith, MAS NMR study of soda-lime-silicate glasses with variable degree of polymerisation, J. Non-Cryst. Solids, 293 (2001) 87-92.

[30] N.J Coleman, 11 Å tobermorite ion exchanger from recycled container glass, Int. J. Environ. Waste Manage. 8 (2011) 366-382.

[31] H. Shao, T.J. Pinnavaia, Synthesis and properties of nanoparticle forms saponite clay, cancrinite zeolite and phase mixtures thereof, Microporous Mesoporous Mater, 133 (2010) 10-17.

[32] K. Mashal, J.B. Harsh, M. Flury, A.R. Felmy, Analysis of precipitates from reactions of hyperalkaline solutions with soluble silica, Appl. Geochem. 20 (2005) 1357-1367.

[33] P. Pena, J.M. Rivas Mercury, A.H. de Aza, X. Turrillas, I. Sobrados, J. Sanz, Solid-state ^{27}Al and ^{29}Si NMR characterization of hydrates formed in calcium aluminate-silica fume mixtures, J. Solid State Chem. 181 (2008) 1744-1752.

[34] G. Engelhardt, D. Michel, High-resolution Solid State NMR of Silicates and Zeolites, first ed. John Wiley & Sons, Chichester, 1987.

[35] J.R. Houston, R.S. Maxwell, S.A. Carroll, Transformation of meta-stable calcium silicate hydrates to tobermorite: reaction kinetics and molecular structure from XRD and NMR spectroscopy, Geochem. Trans. 10:1 (2009) doi:10.1186/1467-4866-10-1

[36] K.A. Cychosz, R. Guillet-Nicolas, J. García-Martínez, M. Thommes, Recent advances in the textural characterization of hierarchically structured nanoporous materials, Chem. Soc. Rev. 46 (2017) 389-414.

[37] M. Murayama, H. Yamamoto, J. Shibata, Synthesis from coal fly ash by hydrothermal reaction using various alkali sources, J. Chem. Technol. Biotechnol. 77 (2002) 280-286.

[38] S. Liu, C. Han, J. Liu, Study of K-feldspar and lime hydrothermal reaction at 190 °C: phase, kinetics and mechanism with reaction time, ChemistrySelect, 3 (2018) 13010-13016.

[39] S.-F. Wong, H. Awala, A. Vincente, R. Retoux, T.C. Ling, S. Mintova, R.R. Mukti, E.P. Ng, K-F zeolite nanocrystals synthesized from organic-template-free precursor mixture, Microporous Mesoporous Mater. 249 (2017) 105-110.

[40] M. Jaishankar, T. Tseten, N. Anbalagan, B.B. Mathew, K.N. Beeregowda, Toxicity, mechanism and health effects of some heavy metals, Interdiscip. Toxicol. 7 (2014) 60-72.

[41] K.K. Wong, C.K. Lee, K.S. Low, M.J. Haron, Removal of Cu and Pb from electroplating wastewater using tartaric acid modified rice husk, Process Biochem. 39 (2003) 437-445.

[42] A. López-Delgado, C. Pérez, F.A. López, Sorption of heavy metals on blast furnace sludge, Water Res. 32 (1998) 989–996.

[43] S. De Gisi, G. Lofrano, M. Grassi, M. Notarnicola, Characteristics and adsorption capacities of low-cost sorbents for wastewater treatment: A review, Sustain. Mater. Technol. 9 (2016) 10-40.

[44] N.J. Coleman, W.E. Lee, I.J. Slipper, Interactions of aqueous Cu^{2+}, Zn^{2+} and Pb^{2+} ions with crushed concrete fines, J. Hazard. Mater. B121 (2005) 203-213.

[45] M.G. Lee, G. Yi, B.J. Ahn, F. Roddick, Conversion of coal fly ash into zeolite and heavy metal removal characteristics of the products, Korean J. Chem. Eng. 17 (2000) 325-331.

[46] X. Querol, N. Moreno, J.C. Umaña, R. Juan, S. Hernández, C. Fernandez-Pereira, D. Cazorla-Amoros, Application of zeolitic material synthesized from fly ash to the decontamination of waste water and flue gas, J. Chem. Technol. Biotechnol. 77 (2002) 292-298.

[47] J. Luo, H. Zhang, J. Yang, Hydrothermal synthesis of sodalite on alkali-activated coal fly ash for removal of lead ions, Procedia Environ. Sci. 31 (2016) 605-614.

[48] W. Qiu, Y. Zheng, Removal of lead, copper, nickel, cobalt, and zinc from water by a cancrinite-type zeolite synthesized from fly ash, Chem. Eng. J. 145 (2009) 483-488.

[49] K. Al-Zboon, M.S. Al-Harahsheh, F. Bani Hani, Fly ash-based geopolymer for Pb removal from aqueous solution, J. Hazard.s Mater. 188 (2011) 414-421.

[50] M. Moshoeshoe, M.S. Nadiye-Tabbiruka, V. Obuseng, A review of the chemistry, structure, properties and applications of zeolites, Am. J. Mater. Sci. 7 (2017) 196-221.

[51] M. Esaifan, L.N. Warr, G. Grathoff, T. Meyer, M.-T. Schafmeister, A. Kruth, H. Testrich, Synthesis of hydroxy-sodalite/cancrinite zeolites from calcite-bearing kaolin for the removal of heavy metal ions in aqueous media, Minerals, 9 (2019) doi:10.3390/min9080484.

[52] M. Golomeova, A. Zendelska, K. Blažev, B. Krstev, B. Golomeov, Removal of heavy metals from aqueous solution using clinoptilolite and stilbite, Int. J. Eng. Res. Technol. 3 (2014) 1029-1035.

[53] A.Q. Selim, L. Sellaoui, S.A. Ahmed, M. Mobarak, E.A. Mohamed, A. Ben Lamine, A. Erto, A. Bonilla-Petriciolet, M.K.Seliem, Statistical physics-based analysis of the adsorption of Cu^{2+} and Zn^{2+} onto synthetic cancrinite in single-compound and binary systems, J. Environ. Chem. Eng. 7 (2019) doi.org/10.1016/j.jece.2019.103217.

[54] V.P. Mallapur, J.U. Kennedy Oubagaranadin, A brief review on the synthesis of zeolites from hazardous wastes, Trans. Indian Ceram. Soc. 76 (2017) doi.org/10.1080/0371750X.2016.1231086.

[55] F. Collins, A. Rozhkovskaya, J.G. Outram, G.J. Millar, A critical review of waste resources, synthesis, and applications for Zeolite LTA, Microporous Mesoporous Mater. 291 (2020) doi.org/10.1016/j.micromeso.2019.109667.

[56] F. Espejel-Ayala, R. Chora Corella, A. Morales Pérez, R. Pérez-Hernández, R.M. Ramírez-Zamora, Carbon dioxide capture utilizing zeolites synthesized with paper sludge and scrap-glass, Waste Manage. Res. 32 (2014) 1219-1226.

[57] T. Takei, H. Ota, Q. Dong, A. Miura, Y. Yonesaki, N. Kumada, H. Takahashi, Preparation of porous material from waste bottle glass by hydrothermal treatment, Ceram. Int. 38 (2012) 2153–2157.

[58] C. Lin, D. Wang, S. Ye, Synthesis of micro-mesoporous glass-analcime composite structure with soda-lime-silica glass as raw material, Funct. Mater. Lett. 12 (2019) doi.org/10.1142/S1793604719500218.

[59] T. Wajima, H. Ishimoto, K. Kuzawa, K. Ito, O. Tamada, M.E. Gunter, J.F. Rakovan, Material conversion from paper sludge ash in NaOH, KOH, and LiOH solution, Am. Mineral. 92 (2007) 1105–1111.

CRediT Roles

Conceptualization - NJC; Data curation - JHT, VKE, APH, NJC; Formal analysis - JHT, VKE, APH, NJC; Funding acquisition - NJC; Investigation - JHT, VKE, APH, NJC; Methodology - JHT, VKE, APH, NJC; Project administration - NJC; Resources - NJC; Software - VKE, APH, NJC; Supervision - NJC; Validation - VKE, APH, NJC; Visualization - VKE, APH, NJC; Roles/Writing - original draft - NJC; Writing - review & editing - VKE, APH, NJC.

Highlights

- Waste amber glass is a suitable feedstock for the synthesis of zeolitic phases

- Feldspathoids and zeolite K-F can be prepared under mild hydrothermal conditions

- Waste glass-derived products can be used as sorbents for Pb^{2+} and Zn^{2+} ions

CRediT Roles

Conceptualization - NJC; Data curation - JHT, VKE, APH, NJC; Formal analysis - JHT, VKE, APH, NJC; Funding acquisition - NJC; Investigation - JHT, VKE, APH, NJC; Methodology - JHT, VKE, APH, NJC; Project administration - NJC; Resources - NJC; Software - VKE, APH, NJC; Supervision - NJC; Validation - VKE, APH, NJC; Visualization - VKE, APH, NJC; Roles/Writing - original draft - NJC; Writing - review & editing - VKE, APH, NJC.

Declaration of interests

☒ The authors declare that they have no known competing financial interests or personal relationships that could have appeared to influence the work reported in this paper.

☐The authors declare the following financial interests/personal relationships which may be considered as potential competing interests: